Supporting Information

Altindis et al. 10.1073/pnas.1721117115

SI Methods

Bioinformatics. The viral genome database (https://www.ncbi.nlm.nih.gov/genome/viruses) was downloaded from the NCBI and was searched for the hormone peptide sequences reported in Table S1 with a threshold e-value ≤0.1 using tBLASTn (50). This yielded the data in Tables S2 and S3. An additional bioinformatics search was performed by BLASTp using the A-chain or B-chain of insulin, IGF1, and IGF2 as query sequences against viral proteomes (NCBI taxonomic ID: 10239). This uncovered GIV VILP presented in this paper, which had not been identified in the original search because the GIV genome was not included in the NCBI viral genome database. The whole protein sequence of each significant hit was compared with insulin, IGF1, and IGF2 using a multiple sequence alignment program (Clustal Omega) to determine the positions of the cysteines and the number of the identical and conserved residues. Sequence alignment was used to predict domain structures of the VILPs, and I-TASSER was used to predict 3D structures (18). SignalP was used to predict the possible signal peptides of the VILPs (www.cbs.dtu.dk/services/SignalP/).

Residues involved in IR and IGF1R binding were added using the CCP4 Molecular Graphics program (www.ccp4.ac.uk/MG/). Crystal structures of human insulin [Protein Data Bank (PDB) ID code 1MSO] and hIGF1R (PDB ID code 1GZR) and I-TASSER–predicted structures of the VILPs were used in this analysis. The two arginines at positions 36 and 37 in the IGF1 molecule are missing from the crystal structure and were inserted manually. An evolutionary tree was constructed using sequences of 30 different insulin, IGF1, and IGF2 sequences and the four VILPs obtained from UniProt (Table S4). After the multiple sequence alignment of these sequences, the alignment file was utilized for the production of a neighbor-joining phylogenetic tree without distance corrections using Clustal Omega (https://www.ebi.ac.uk/Tools/msa/clustalo/).

The sequences identified in the previously published enteric virome/microbiome analysis were used to make a blast database. SGIV, GIV, LCDV-Sa, and LCDV-1 genomes were used as queries for search against the library using the BLASTn program to determine if these viruses are present in these samples. The significant hits obtained from the virome/microbiome study for VILP-carrying viruses were explored a second time to determine their specificity to these viruses and to show they are not found in any other species. The significant DNA reads were retrieved from the previous BLAST databases result and were used as queries to run BLASTn on the NCBI nonredundant database. The sequences reported in this study are the ones that are 100% specific to these viruses. The code for these database searches is available at https://github.com/jdreyf/viral-insulin-peptides.

Peptide Synthesis and Folding. The single-chain viral insulins were assembled on 0.1 mmol Rink amide ChemMatrix (PCAS BioMatrix Inc.) resin using an ABI 433A peptide synthesizer and Fmoc/6-Cl-HOBt/*N*,*N*′-diisopropylcarbodiimide coupling protocols. Fmoc-Asp-OtBu was employed to introduce the C-terminal Asn. Cleavage was conducted by treatment with 10 mL of trifluoroacetic acid (TFA) solution containing 2.5% triisopropylsilane, 2.5% 2-mercaptoethanol, 2.5% anisole, and 2.5% H_2O at room temperature with gentle agitation for 2 h. The resin was filtered, and the peptide was precipitated by the addition of cold ether (50 mL). The precipitate was collected by centrifugation and then was washed with cold ether (3 × 50 mL). The crude peptide was dissolved in 20 mM alkaline glycine buffer (500 mL) followed with the addition of solid cysteine·HCl (0.75 mmol). The pH of the solution was adjusted to 10.5 with 1 M NaOH. Sonication was used to accelerate the dissolution of the crude peptide. The resulting solution was stirred vigorously at 4 °C for 2 d. The pH was lowered to 7.0 by the addition of 1 M HCl, and the solution was subjected to purification by preparative reverse-phase HPLC column [Luna 10-μm C8 100 Å, LC column (Phenomenex Inc.), 250 × 21.2 mm, 10–50% aqueous acetonitrile (0.1% TFA) over 90 min, at a flow rate of 15 mL/min]. The results were assessed by analytical LC-MS. The pooled fractions were lyophilized to provide the single-chain viral insulin as a white fluffy solid.

Receptor Competition Assays. Murine brown preadipocyte cell lines with double knockout of the endogenous IR and IGF1R were stably transfected with either hIR-B or hIGF1R, as previously described (25), and were grown to confluence in 48-well plates and were serum-starved overnight. After washing with PBS, cells were incubated in a Hepes binding buffer containing ^{125}I-IGF1 (2.5 nM) for hIGF1R-binding experiments or ^{125}I-insulin (1 nM) for IR-binding experiments and increasing concentrations of the unlabeled ligands for 2 h at room temperature. Binding competition was performed in triplicate for each dose. After washing, cells were solubilized with 0.1 M NaOH containing 0.1% SDS, and radioactivity was measured using a gamma-counter. The data were plotted as the percentage of the maximal binding of the ligand alone and were expressed as mean ± SEM.

IR and IGF1R Phosphorylation. HEK293 cells (ATCC CRL-1573) overexpressing hIR-A, hIR-B, or hIGF1R were plated in 96-well plates and were cultured in DMEM supplemented with 100 IU/mL penicillin, 100 μg/mL streptomycin, 10 mM Hepes, and 0.25% bovine growth serum (HyClone SH30541) for 16–20 h at 37 °C, 5% CO_2, and 90% humidity. Serial dilutions of recombinant human insulin, IGF1, and test peptides were prepared in DMEM supplemented with 0.5% BSA and were added to the wells. After 15 min incubation at 37 °C in humidified atmosphere with 5% CO_2, the cells were fixed with 5% paraformaldehyde for 20 min at room temperature, washed twice with PBS (pH 7.4), and blocked with 2% BSA in PBS for 1 h. The plate was washed three times, filled with HRP-conjugated antibody against phosphotyrosine (#16-105; Upstate Biotechnology), and incubated for 3 h at room temperature, after which the plate was washed four times, and 0.1 mL of TMB One-Solution substrate (#00-2023; Invitrogen) was added to each well. Color development was stopped 5 min later by adding 0.05 mL 1 M HCl. Absorbance at 450 nm was measured on a Titertek Multiskan MCC340 microplate reader (Thermo Fisher). Absorbance vs. peptide concentration dose–response curves were plotted, and EC_{50} values were determined using logistic nonlinear three-parameter regression in GraphPad Prism 6 (GraphPad Software).

Insulin Signaling and Immunoblotting. All cells were maintained in DMEM supplemented with 10% FBS, 100 U/mL penicillin, and 100 μg/mL streptomycin (Gibco) and were cultured at 37 °C in a humidified atmosphere of 5% CO_2. Cells expressing hIR-B, mIR-A, hIGF1R, and mIGF1R were serum-starved for 4 h with DMEM containing 0.1% BSA and were stimulated with insulin, IGF1, or VILPs at the indicated concentrations for 15 or 60 min as indicated in Fig. 2 *F* and *H* and Fig. S4. To stop the experiments, cells were washed with ice-cold PBS and were lysed with RIPA lysis buffer (Millipore) complemented with 50 mM

potassium fluoride, 50 mM β-glycerolphosphate, 2 mM EGTA (pH 8), 1 mM Na_3VO_4, and 1× protease inhibitor mixture (Calbiochem). Protein concentrations were determined using the Pierce 660 nm Protein Assay Reagent (Bio-Rad). Lysates (10–20 μg) were resolved on SDS/PAGE gels and were transferred to PVDF membrane for immunoblotting. Membranes were blocked in Starting Block T20 (Thermo Fisher) at room temperature for 1 h, were incubated with the indicated primary antibody in Starting Block T20 solution overnight at 4 °C (Figs. 2 and 3 and Fig. S4), and then were washed three times with 1× PBS and Tween-20 and incubated with HRP-conjugated secondary antibody (1:20,000; anti-mouse IgG, NA931; anti-rabbit IgG, NA934; GE Healthcare) in Starting Block T20 for 1 h. Signals were detected using Immobilon Western Chemiluminescent HRP Substrate (Millipore). Antibodies against phospho-IR/IGF1R (1:500; #3024), IRβ (1:500; sc-711), phospho-ERK1/2 (T202/Y204) (1:1,000; #9101), ERK1/2 (1:1,000; #9102), phospho-Akt (S473) (1:1,000; #9271), and Akt (1:1,000; #4685) were purchased from Cell Signaling Technologies. IRβ antibody (1:500; sc-711) was purchased from Santa Cruz. Human insulin was purchased from Sigma, and hIGF1 was purchased from PeproTech. Densitometric analyses of membranes were performed using ImageJ.

Plasmid Transfections. The cDNA sequence of the LCDV-1 VILP gene (240 bp, whole sequence) was synthesized by Integrated DNA Technologies, Inc. and was subcloned into 3×Flag-CMV-10 mammalian expression vector (Sigma). For transfection, AML-12 (mouse hepatocyte cell line; ATCC) cells were plated at 5×10^4 cells per well and were transfected using 1 μL of Lipofectamine 3000 and 0.5 μg DNA for 0.3 mL medium in each well per the manufacturer's instructions. For signaling experiments of LCDV-1 VILP-transfected cells, the culture medium was replaced 12 h after the transfections with starvation medium (DMEM containing 0.1% BSA), and cells were incubated for an additional 24 h.

DNA Synthesis and Proliferation. GM00409 human fibroblasts (Coriell Institute) were plated in 24-well plates at 5×10^4 cells per well in 500 μL DMEM supplemented with 10% FBS, 100 U/mL penicillin, and 100 μg/mL streptomycin (Gibco) and were cultured at 37 °C in a humidified atmosphere of 5% CO_2. After 24-h incubation, the cells were serum-starved for 24 h with DMEM containing 0.1% BSA, after which 1 μCi [^{3}H]-thymidine (Perkin-Elmer) was added to each well along with the indicated concentrations of ligands, all in triplicate. Experiments were stopped after 24 h, and the wells were washed with PBS. Cells were fixed by the addition of 10% trichloroacetic acid (TCA) for 10 min and were incubated at −20 °C. The plates were washed one more time with 10% TCA and were lysed in 0.1 M NaOH, followed by liquid scintillation counting.

For transfected AML-12 cells, a related protocol was used. Twelve hours after transfection, cells were serum-starved for 3 h with DMEM containing 0.1% BSA, and 1 μCi [^{3}H]-thymidine was added. The experiment was stopped after 6 h of incubation with thymidine.

Cell Culture and Glucose Uptake. 3T3-L1 cells were differentiated as described previously (51). For 2-deoxyglucose uptake, cells were washed with PBS and incubated in starvation medium (low-glucose DMEM + 0.5% FBS) at 37 °C. After 3-h incubation, cells were washed again with PBS, and 0.45 mL of Krebs–Ringer Hepes buffer (KRBH) was added with the indicated concentrations of insulin, IGF1, or different viral insulins for 30 min at 37 °C. One microcurie of [^{14}C] 2-deoxyglucose (Sigma) in 50 μL KRBH was added to each well for the final 5 min of stimulation. Glucose uptake was stopped by adding 50 μL of 200 mM 2-deoxyglucose. Cells were washed with PBS and were lysed with lysis buffer (0.1% SDS in PBS) followed by liquid scintillation counting. For Fig. 4*A*, results of two experiments were combined.

Insulin Tolerance Test. All animal studies complied with the regulations and ethics guidelines of the NIH and were approved by the Institutional Animal Care and Use Committees of the Joslin Diabetes Center (no. 97-05) and Harvard Medical School (no. 05131). I.p. insulin tolerance testing was performed after a 4-h fast using 9-wk-old male C57BL/6J mice (Jackson Laboratory). Mice were injected i.p with LCDV-1 VILP (1 μmol/kg; $n = 4$), SGIV VILP (1 μmol/kg; $n = 4$), insulin [Humulin, 6 nmol/kg (1.0 U/kg); $n = 6$], or 200 μL of saline ($n = 6$). Tail-vein blood glucose was measured at the indicated time points (Fig. 4*B*) using an Infinity glucometer (US Diagnostics Inc.). Statistical analysis was by two-way ANOVA followed by Tukey correction; $^*P < 0.05$; $^{**}P < 0.01$, $^{****}P < 0.0001$.

Data and Code Availability. The VILP structures were predicted using I-TASSER (https://zhanglab.ccmb.med.umich.edu/I-TASSER/). All the data used in this study, including PDB files and all the original codes that support the bioinformatics analysis in this study have been deposited with GitHub, https://github.com/jdreyf/viral-insulin-peptides.

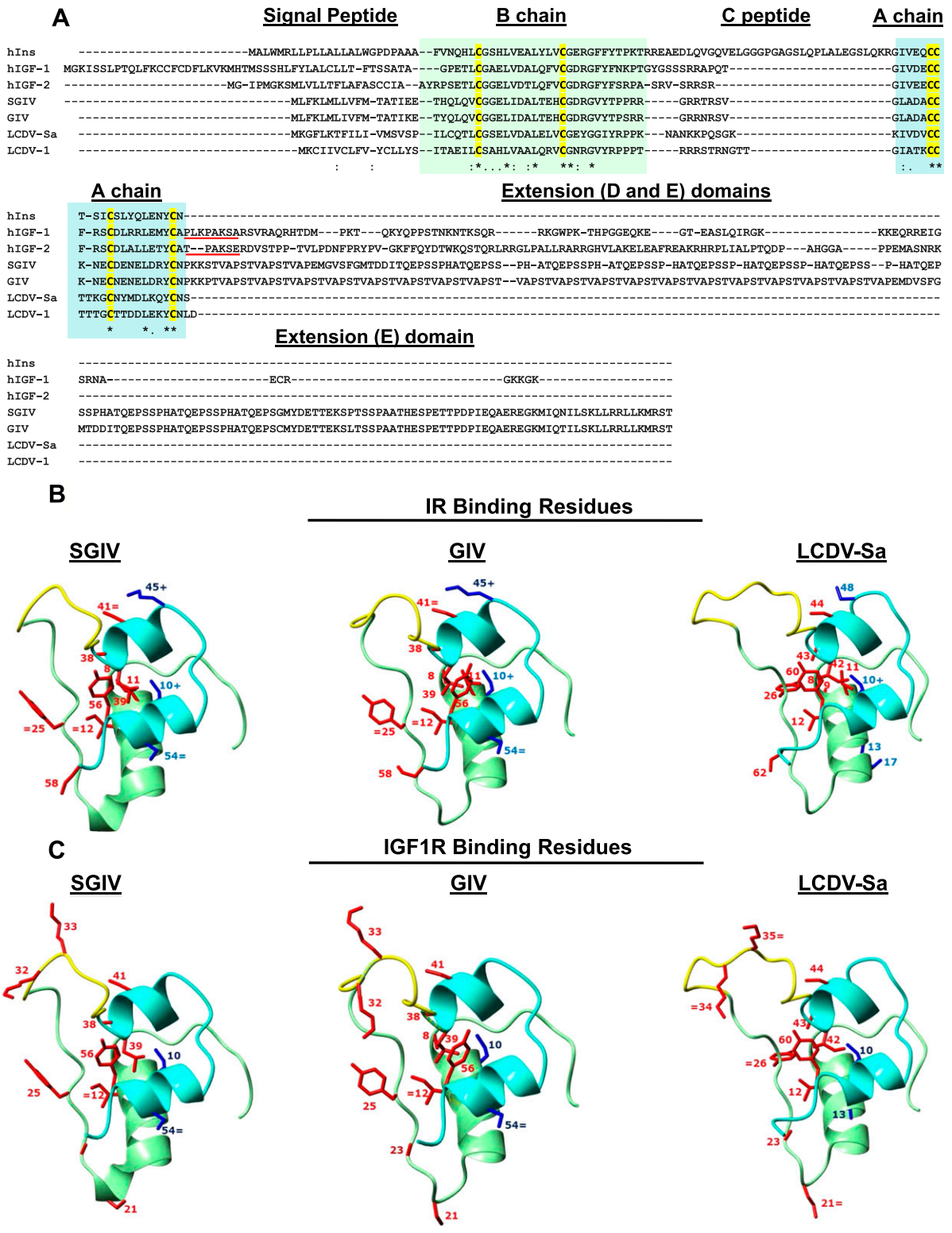

Fig. S1. VILPs are structurally a part of insulin superfamily. (*A*) Whole-sequence alignment of insulin, IGF1, IGF2, and four VILPs. The domains are shown at the top of the sequences. Identical residues are denoted by asterisks, and low and high degrees of similarity are represented by periods and colons, respectively. The underlined sequences are D-domains of IGF1 and IGF2. (*B* and *C*) Conservation IR- (*B*) and IGF1R- (*C*) binding residues of VILPs. The I-TASSER–predicted structures of SGIV, GIV, and LCDV-Sa are shown. The A-chain is cyan; the B-chain is light green; the C-peptide is yellow; and the D-domain is pale brown. The conserved or conservatively substituted side chains of residues of VILPs that are involved in binding to site 1 of the IR/IGF1R are shown in red, and binding-site 2 residues are shown in blue. Conservative substitutions are also indicated by an equal sign. Substitutions that increase affinity are indicated by a plus sign. Molecules were drawn with CCP4-Molecular Graphics.

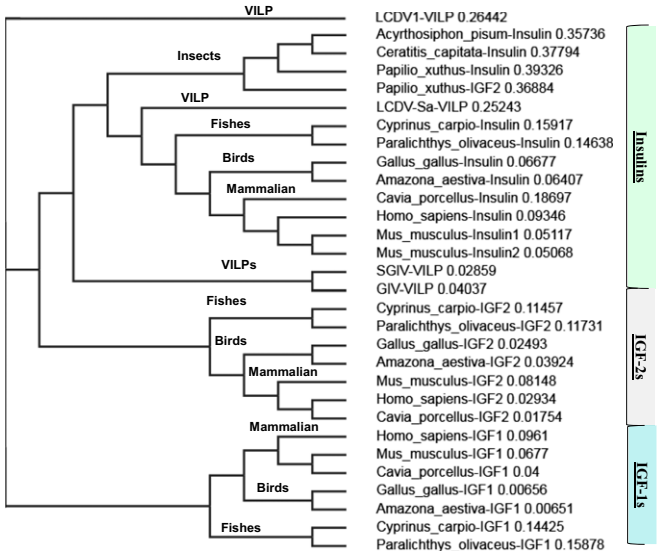

Fig. S2. Phylogenetic tree for VILPs. A phylogenetic tree produced by Clustal Omega for a sample of 30 vertebrate sequences, including fish, insect, mammal, and bird insulins, IGF1s, IGF2s, and VILPs. The numbers are the terminal branch distances, the distance since the last theoretical splitting event.

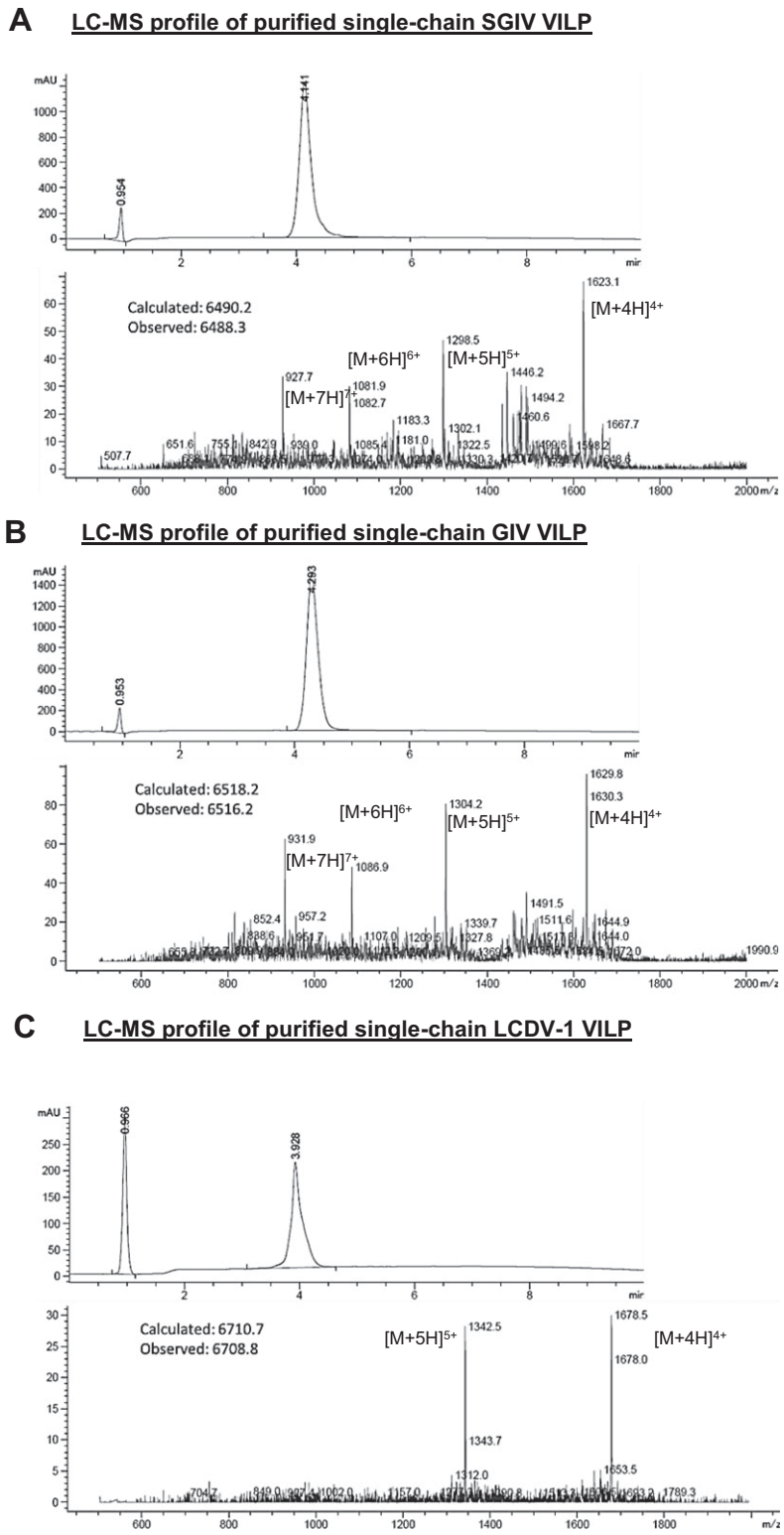

Fig. S3. LC-MS profile of purified single-chain VILPs. Each panel shows the LC-MS profile of a purified VILP. (*A*) SGIV. The single-chain peptide eluted at 4.141 min as a single peak. A mass of 6,488.3 was found for the peptide, consistent with the calculated molecular weight of 6,490.2. (*B*) GIV. The single-chain peptide eluted at 4.293 min as a single peak. A mass of 6,518.2 was found for the material, consistent with the calculated molecular weight of 6,516.2. (*C*) LCDV-1. The single-chain peptide eluted at 3.928 min as a single peak. A mass of 6,710.7 was found for the material, consistent with the calculated molecular weight of 6,708.8.

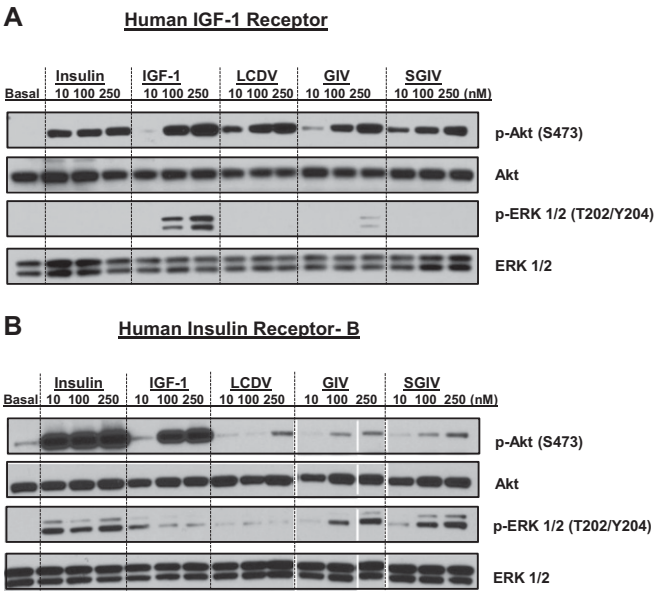

Fig. S4. SGIV and GIV stimulate a late postreceptor signaling response. (*A*) Immunoblotting of protein phosphorylation in lysates from hIGF1R-overexpressing cells stimulated with insulin, IGF1, or VILPs for 60 min. (*B*) Immunoblotting of protein phosphorylation in lysates from hIR-overexpressing cells stimulated with insulin, IGF1, or VILPs for 60 min. Because of an error in the loading order for the different concentrations of GIV, the image showing stimulation in cells overexpressing hIR has been cut and rearranged to indicate a dose–response similar to other analogs. The areas of cutting are indicated by the vertical white lines in the figure.

Table S1. SignalP-predicted signal peptide positions of the VILPs

VILP source	Signal peptide	Cleavage site position	Residues
SGIV VILP	Yes	Between positions 20 and 21	THQ-LQ
GIV VILP	Yes	Between positions 20 and 21	TYQ-LQ
LCDV-1 VILP	Yes	Between positions 19 and 20	ITA-EI
LCDV-Sa VILP	Yes	Between positions 20 and 21	ILC-QT

Table S2. hIR-binding site 1 and corresponding residues on hIGF1 and VILPs

hIR-binding site 1	Human insulin	Ala mutation, K%	hIGF1	GIV	SGIV	LCDV-1	LCDV-Sa
B8	GLY	0.8	GLY 7	GLY 8	GLY 8	SER 8	GLY 8
B9	SER	72	ALA 8	GLY 9	GLY 9	ALA 9	SER 9
B11	LEU	3	LEU 10	LEU 11	LEU 11	LEU 11	LEU 11
B12	VAL	1	VAL 11	ILE 12	ILE 12	VAL 12	VAL 12
B16	TYR	34	GLN 15	THR 16	THR 16	GLN16	GLU 16
B24	PHE	5	PHE 23	VAL 24	VAL 24	VAL 24	GLY 24
B25	PHE	10	TYR 24	TYR 25	TYR 25	TYR 25	THR 25
B26	TYR	100	PHE 25	THR 26	THR 26	ARG 26	TYR 26
A1	GLY	12	GLY 42	GLY 38	GLY 38	GLY 41	LYS 41
A2	ILE	0.6	ILE 43	LEU 39	LEU 39	ILE 42	ILE 42
A3	VAL	1.8	VAL 44	ALA 40	ALA 40	ALA 43	VAL 43
A4	GLU	142	ASP 45	ASP 41	ASP 41	THR 44	ASP 44
A19	TYR	<0.1	TYR 60	TYR 56	TYR 56	TYR 60	TYR 60
A21	ASN	63	ALA 62	ASN 58	ASN 58	ASN 62	ASN 62

Column 3 shows the effect of alanine ligand mutations on the hIR-binding affinity (from ref. 14 and references therein). Residue numbering is according to the corresponding PDB ID codes. Underlined residues are neither conserved nor conservatively substituted.

Table S3. hIR-binding site 2 and corresponding residues on hIGF1 and VILPs

hIR-binding site 2	Human insulin	Ala mutation, K%	hIGF-1	GIV	SGIV	LCDV-1	LCDV-Sa
B10	HIS	37	GLU 9	GLU 10	GLU 10	HIS 10	GLU 10
B13	GLU	10	ASP 12	ASP 13	ASP 13	ALA 13	ASP 13
B17	LEU	23	PHE 16	GLU 17	GLU 17	ARG 17	LEU 17
A8	THR	40	PHE 49	LYS 45	LYS 45	THR 48	THR 48
A10	ILE	20	SER 51	GLU 47	GLU 47	GLY 51	GLY 51
A12	SER	36	ASP 53	ASP 49	ASP 49	THR 53	ASN 53
A13	LEU	15	LEU 54	GLU 50	GLU 50	THR 54	TYR 54
A17	GLU	35	GLU 58	ASP 54	ASP 54	GLU 58	LYS 58

Column 3 shows the effect of alanine ligand mutations on the hIR-binding affinity (from ref. 14 and references therein). Residue numbering is according to the corresponding PDB ID codes. Underlined residues are neither conserved nor conservatively substituted.

Table S4. hIGF1R-binding site 1 residues and corresponding residues on human insulin and VILPs

hIGF1R-binding site 1	Ala mutation, K%	Insulin	GIV	SGIV	LCDV-1	LCDV-Sa
GLY 7		GLY B8	GLY 8	GLY 8	SER 8	GLY 8
ALA 8		SER B9	GLY 9	GLY 9	ALA 9	SER 9
VAL 11	40	VAL B12	ILE 12	ILE 12	VAL 12	VAL 12
ASP 20		GLU B21	ASP 21	ASP 21	ASN 21	GLU 21
GLY 22		GLY B23	GLY 23	GLY 23	GLY 23	GLY 23
PHE 23		PHE B24	VAL 24	VAL 24	VAL 24	GLY 24
TYR 24		PHE B25	TYR 25	TYR 25	TYR 25	THR 25
PHE 25		TYR B26	THR 26	THR 26	ARG 26	TYR 26
TYR 31	17	-	GLY 31	GLY 31	ARG 31	ALA 31
ARG 36	7 (36 + 37)	-	ARG 32	ARG 32	ARG 32	LYS 34
ARG 37		-	ARG 33	ARG 33	ARG 33	LYS 35
GLY 42		GLY A1	GLY 38	GLY 38	GLY 41	LYS 41
ILE 43		ILE A2	LEU 39	LEU 39	ILE 42	ILE 42
VAL 44		VAL A3	ALA 40	ALA 40	ALA 43	VAL 43
ASP 45		GLU A4	ASP 41	ASP 41	THR 44	ASP 44
MET 59		ASN A18	ARG 55	ARG 55	LYS 59	ASN 59
TYR 60		TYR A19	TYR 56	TYR 56	TYR 60	TYR 60

Column 2 shows the effect of alanine ligand mutations on the IGF-1R affinity (from refs. 15 and 16 and references therein). Residue numbering is according to the corresponding PDB ID codes. Underlined residues are neither conserved nor conservatively substituted. The affinity of alanine mutation at residues 36 and 37 is a combined mutation at both sites.

Table S5. hIGF1R-binding site 2 residues and corresponding residues on human insulin and VILPs

hIGF1R-binding site 2	Ala mutation, K%	Insulin	GIV	SGIV	LCDV-1	LCDV-Sa
GLU 9	34	HIS B10	GLU 10	GLU 10	HIS 10	GLU 10
ASP 12	29	GLU B13	ASP 13	ASP 13	ALA 13	ASP 13
PHE 16	50	LEU B17	GLU 17	GLU 17	ARG 17	LEU 17
LEU 54	24	LEU A13	GLU 52	GLU 52	THR 53	TYR 53
GLU 58	15	GLU A17	ASP 54	ASP 54	GLU 58	LYS 58

Column 2 shows the effect of alanine ligand mutations on the IGF-1R affinity (from refs. 15 and 16 and references therein). Residue numbering is according to the corresponding PDB ID codes. Underlined residues are neither conserved nor conservatively substituted. The affinity of alanine mutation at residues 36 and 37 is a combined mutation at both sites.

Table S6. Insulin, IGF1, IGF2, and VILP sequences used to produce the Clustal Omega phylogenetic tree

VILP source	Sequence
Human insulin	MALWMRLLPLLALLALWGPDPAAAFVNQHLCGSHLVEALYLVCGERGFFYTPKTRREAED LQVGQVELGGGPGAGSLQPLALEGSLQKRGIVEQCCTSICSLYQLENYCN
Human IGF1	MGKISSLPTQLFKCCFCDFLKVKMHTMSSSHLFYLALCLLTFTSSATAGPETLCGAELVD ALQFVCGDRGFYFNKPTGYGSSSRRAPQTGIVDECCFRSCDLRRLEMYCAPLKPAKSARS VRAQRHTDMPKTQKYQPPSTNKNTKSQRRKGWPKTHPGGEQKEGTEASLQIRGKKKEQRR EIGSRNAECRGKKGK
Human IGF2	MGIPMGKSMLVLLTFLAFASCCIAAYRPSETLCGGELVDTLQFVCGDRGFYFSRPASRVS RRSRGIVEECCFRSCDLALLETYCATPAKSERDVSTPPTVLPDNFPRYPVGKFFQYDTWK QSTQRLRRGLPALLRARRGHVLAKELEAFREAKRHRPLIALPTQDPAHGGAPPEMASNRK
Cyprinus carpio insulin	MAVWIQAGALLFLLAVSSVNANAGAPQHLCGSHLVDALYLVCGPTGFFYNPKRDVDPPLG FLPPKSAQETEVADFAFKDHAEVIRKRGIVEQCCHKPCSIFELQNYCN
Cyprinus carpio IGF1	KCTMRCLSCTHTLSLVLCVLALTPATLEAGPETLCGAELVDTLQFVCGDRGFYFSKPTGY GPSSRRSHNRGIVDECCFQSCELRRLEMYCAPVKPGKTPRSVRAQRHTDSPRTAKKPLPG QSHSSYKEVHQKNS
Cyprinus carpio IGF2	MEDQLKHHSLCHTCLRTDSVINKVIKMYWSIRMPICILFLTLSAFEVASAETLCGGELVD ALQFVCGDRGFYFSRPTSRLSSRRSQNRGIVEECCFNSCNLALLEQYCAKPAKSERDVSA TSLQVIPVMPTLKQEVPRKHVTVKYSKYDMWQRKAAQRLRRGVPAILRAKKFRRQAERIR AQEQLHHHRPLITLPSKLPPILFAQSR
Paralichthys olivaceus insulin	MAALWLHSVSLLVLLIVSLPASSQAMAPPQHLCGAHLVDALYLVCGERGFFYTPKRDVDP LLGFLPPKSGGAAAGGENEVAEFAFKDQMEMMVKRGIVEQCCHKPCNIFDLQNYCN
Paralichthys olivaceus IGF1	MSSALSFQWHLCDVFKSAMCCISCSHTLSLLLCVLTLTPTATGAGPETLCGAELVDTLQF VCGERGFYFSKPTGYGPNARRSRGIVDECCFQSCELRRLEMYCAPAKTSKAARSVRAQRH TDMPRAPKVSTAGHKVDKGTERRTAQQPDKTKNKKRPLPGHSHTHALLFMRQSQLLTFCV GIVCE
Paralichthys olivaceus IGF2	METQKRHGQHSLCHTCRRAESSRLKVKKMSSSSRALLFALALTLYVVEMASAETLCGGEL VDALQFVCEDRGFYFSRPTSRGSNRRPQNRGIVEECCFRSCDLNLLEQYCAKPAKSERDV SATSLQVIPVMPALKQEVPRKQHVTVKYSKYEVWQRKAAQRLRRGVPAILRAKKFRRQAE KIKAQEQAIFHRPLISLPSKLPPVLLATDNYVNHN
Mus musculus insulin 1	MALLVHFLPLLALLALWEPKPTQAFVKQHLCGPHLVEALYLVCGERGFFYTPKSRREVED PQVEQLELGGSPGDLQTLALEVARQKRGIVDQCCTSICSLYQLENYCN
Mus musculus insulin2	MALWMRFLPLLALLFLWESHPTQAFVKQHLCGSHLVEALYLVCGERGFFYTPMSRREVED PQVAQLELGGGPGAGDLQTLALEVAQQKRGIVDQCCTSICSLYQLENYCN
Mus musculus IGF1	MGKISSLPTQLFKICLCDFLKIKIHIMSSSHLFYLALCLLTFTSSTTAGPETLCGAELVD ALQFVCGPRGFYFNKPTGYGSSIRRAPQTGIVDECCFRSCDLRRLEMYCAPLKPTKAARS IRAQRHTDMPKTQKEVHLKNTSRGSAGNKTYRM
Mus musculus IGF2	MGIPVGKSMLVLLISLAFALCCIAAYGPGETLCGGELVDTLQFVCSDRGFYFSRPSSRAN RRSRGIVEECCFRSCDLALLETYCATPAKSERDVSTSQAVLPDDFPRYPVGKFFQYDTWR QSAGRLRRGLPALLRARRGRMLAKELKEFREAKRHRPLIVLPPKDPAHGGASSEMSSNHQ
Gallus gallus insulin	MALWIRSLPLLALLVFSGPGTSYAAANQHLCGSHLVEALYLVCGERGFFYSPKARRDVEQ PLVSSPLRGEAGVLPFQQEEYEKVKRGIVEQCCHNTCSLYQLENYCN
Gallus gallus IGF1	MEKINSLSTQLVKCCFCDFLKVKMHTVSYIHFFYLGLCLLTLTSSAAAGPETLCGAELVD ALQFVCGDRGFYFSKPTGYGSSSRRLHHKGIVDECCFQSCDLRRLEMYCAPIKPPKSARS VRAQRHTDMPKAQKEVHLKNTSRGNTGNRNYRM
Gallus gallus IGF2	MEKINSLSTQLVKCCFCDFLKVKMHTVSYIHFFYLGLCLLTLTSSAAAGPETLCGAELVD ALQFVCGDRGFYFSKPTGYGSSSRRLHHKGIVDECCFQSCDLRRLEMYCAPIKPPKSARS VRAQRHTDMPKAQKEVHLKNTSRGNTGNRNYRM
Amazona aestiva insulin	MALWILSLPLLALLALSGPXTSHAAATQHLCGSHLVEALYLVCGERGFFYSPKARRDVEQ PLVSGRLHGEVGELPFQPEEFQKVKRGIVEQCCHNTCSLYQLENYCN
Amazona aestiva IGF1	MEKINSLSTQLVKCCLCDFLKVKMHTVSYIHFFYLGLCLLTLTSSAAAGPETLCGAELVD ALQFVCGDRGFYFSKPTGYGSSSRRLHHKGIVDECCFQSCDLRRLEMYCAPIKPPKSARS VRAQRHTDMPKAQKEVHLKNSSRGNTGNRNYRM
Amazona aestiva IGF2	MSSAGAHTDERCRQPAFLPGPPPPPEVESSSGSSKVQRMCAARRMMLLLLAFLAYALDSA AAYGTAETLCGGELVDTLQFVCGDRGFYFSRPVGRNNRRINRGIVEECCFRSCDLALLET YCAKSVKSERDLSATSLAGLPALSKESFQKPSHAKYSKYDVWQKKSSQRLQREVPGILRA RQYRWQAEGLQAAEEAKALHRPLISLPSQRPPAARASPETAGPQK
Papilio xuthus insulin	MCLSRVQGELDNVFSLHVMHCFIEIKTSEKISKMKLIICIMATGILFGNVSTNISFEDGK AMHFCGRTLIDALILLCNMEETHLSAEVQPSEQYIVKNTLNEMKANYKDIKSKLSRRQKR DLVDTCCYKPCKYEDLRMYC
Papilio xuthus IGF2	MLLRRVVTALLAVAAGAALCGRADAASVAMKLCGRKLGEILSRVCSAYNSPAWDVPTVVE QTAGVVRRRRETGIVYECCTQGCTLEHLTEYCATTIKATSETSVDSHMIEDRSAESTGSG STGAAGAAGMATAARAPAAHIIKSAARAAPVVGTVSPLLTWGRTLNTDLPTVDNDRYAYV IYA

Table S6. Cont.

VILP source	Sequence
Acyrthosiphon pisum insulin	MKISMYLSVILLALVIKVVTANVRLQRSPQQYCGSKLADIMKALCNTKYNVPKGHKRSEI DFDVWDYKDLEDYNAVDYPYIKKEDISFMPSRFRRSVKRSIIDECCRRPCYLSELKSYCA SQ
Ceratitis capitata insulin	MKFPEQTLSFPNLLCLSFVVISLVFCVELSPHCTEALPLLPGGSTEVEFKRYCSTNLSDA IRLICGGRYYSLSRKFPDSVGMAQVSSLKRLAGEDGEYRQPFQGAIHECCRRPCGYSELK SYCDPDY
Cavia porcellus insulin	MALWMHLLTVLALLALWGPNTGQAFVSRHLCGSNLVETLYSVCQDDGFFYIPKDRRELED PQVEQTELGMGLGAGGLQPLALEMALQKRGIVDQCCTGTCTRHQLQSYCN
Cavia porcellus IGF1	MHAVSSSHLFYLAFCLLVLTSSATAGPETLCGAELVDALQFVCGDRGFYFNKPTGYGSSS RRAPQTGIVDECCFRSCDLRRLEMYCAPLKPAKSARSVRAQRHTDMPKTQKEVHLKNASR GSAGNKNYRM
Cavia porcellus IGF2	MGISMGKSMLVLLTFLAFASCCIAAYRPSETLCGGELVDTLQFVCGDRGFYFSRPASRVS RRSRGIVEECCFRSCDLALLETYCATPAKSERDVSASLAVLPDNFPRYPVGKFFQYDTWR QSTQRLRR
SGIV-VILP	THQLQVCGGELIDALTEHCGDRGVYTPPRRGRRTRSVGLADACCKNECDENELDRYCN
GIV-VILP	TYQLQVCGGELIDALTEHCGDRGVYTPSRRGRRNRSVGLADACCKNECNENELDRYCN
LCDV1-VILP	ITAEILCSAHLVAALQRVCGNRGVYRPPPTRRRSTRNGTTGIATKCCTTTGCTTDDLEKYCN
LCDV-Sa-VILP	ILCQTLCGSELVDALELVCGEYGGIYRPPKNANKKPQSGKKIVDVCCTTKGCNYMDLKQYCN

Table S7. Approximate EC_{50} values (nM) calculated for the autophosphorylation experiment

Receptor	Human insulin	hIGF-1	GIV	SGIV	LCDV-1
hIGF1R	41	0.9	438	92	11
hIR-A	0.51	8	2,063	745	484
hIR-B	0.65	39	4,208	3,510	2,787

Other Supporting Information Files

Dataset S1 (PDF)
Dataset S2 (PDF)
Dataset S3 (PDF)
Dataset S4 (PDF)
Dataset S5 (PDF)
Dataset S6 (PDF)